

Thermodynamic uncertainty relation in nondegenerate and degenerate maser heat engines

Varinder Singh ^{1,*} Vahid Shaghaghi ^{1,2,3} Özgür E. Müstecaplıoğlu ^{4,5} and Dario Rosa ^{1,6}

¹*Center for Theoretical Physics of Complex Systems, Institute for Basic Science, Daejeon 34126, Korea*

²*Center for Nonlinear and Complex Systems, Dipartimento di Scienza e Alta Tecnologia, Università degli Studi dell'Insubria, via Valleggio 11, 22100 Como, Italy*

³*Istituto Nazionale di Fisica Nucleare, Sezione di Milano, via Celoria 16, 20133 Milano, Italy*

⁴*Department of Physics, Koç University, 34450 Sarıyer, Istanbul, Turkey*

⁵*TÜBİTAK Research Institute for Fundamental Sciences, 41470 Gebze, Turkey*

⁶*Basic Science Program, Korea University of Science and Technology, Daejeon 34113, Korea*



(Received 25 December 2022; accepted 15 August 2023; published 5 September 2023)

We investigate the thermodynamic uncertainty relation (TUR), i.e., a tradeoff between entropy production rate and relative power fluctuations, for nondegenerate three-level and degenerate four-level maser heat engines. In the nondegenerate case, we consider two slightly different configurations of the three-level maser heat engine and contrast their degree of violation of the standard TUR. We associate their different TUR-violating properties to the phenomenon of spontaneous emission, which gives rise to an asymmetry between them. Furthermore, in the high-temperature limit, we show that the standard TUR relation is always violated for both configurations. For the degenerate four-level engine, we study the effects of noise-induced coherence on the TUR. We show that, depending on the parametric regime of operation, noise-induced coherence can either suppress or amplify the relative power fluctuations.

DOI: [10.1103/PhysRevA.108.032203](https://doi.org/10.1103/PhysRevA.108.032203)

I. INTRODUCTION

Since the dawn of the industrial revolution, heat engines have played an important role in the development of classical thermodynamics on both theoretical and experimental fronts. Even with the rise of quantum thermodynamics [1–7]—which extends the study of heat and work to the quantum regime—heat engines remain among the central research topics. In order to harness quantum resources such as entanglement, coherence, and quantum fuels to our advantage (which is at the heart of the flourishing area of quantum technologies), it is important to understand the energy conversion process at the nanoscale. However, thermal machines operating at the nanoscale are subject to thermal as well as quantum fluctuations due to their small size, which may negatively affect their performance. Hence, it is crucial to develop a fundamental understanding of these fluctuations characterizing the performance of quantum thermal machines. Recently, a conceptual advance has been made in this direction by Barato and Seifert [8] by introducing the thermodynamic uncertainty relation (TUR). In the context of steady-state classical heat engines, the TUR states that there is always a tradeoff between the relative fluctuation in the power output and the thermodynamic cost (rate of entropy production $\langle\sigma\rangle$) of maintaining the nonequilibrium steady state (in the following, we will work in units having $\hbar = k_B = 1$):

$$\mathcal{Q} \equiv \langle\sigma\rangle \frac{\Delta P}{\langle P\rangle^2} \geq 2, \quad (1)$$

where $\langle P\rangle$ denotes the mean power of the engine while $\Delta P = \lim_{t \rightarrow \infty} \langle [P(t) - \langle P\rangle]^2 \rangle t$ is the rescaled variance of the power in the steady state. Finally, $P(t)$ is the power averaged from time $t = 0$ to t [9–13]. Equation (1) was originally discovered for biomolecular processes [8] and proved by using the formalism of large deviation theory [14].

The original TUR, Eq. (1), which we will refer to as the standard thermodynamic uncertainty relation (STUR) from now on, is applicable to systems in nonequilibrium steady state obeying a Markovian continuous-time dynamics with explicit time-independent driving [15]. Later, it was shown to hold in finite time [16,17]. Without any one of the assumptions mentioned above, Eq. (1) can be violated [15]. Thus, a number of generalizations have been proposed in various settings [9,18–43]. Additionally, there has been a considerable amount of effort to probe the validity and extensions of the STUR in quantum systems [10,11,44–65].

Recently, the role of quantum coherence in the violations of TURs has been explored in detail [66,67]. Specifically, it has been shown that fluctuations are not encoded in the steady state alone and STUR violations can be seen as the consequence of coherent dynamics going beyond steady-state coherence [66,67]. In these papers, attention is put on the effect of drive-induced coherence on TURs. On the other hand, the effect of *noise-induced coherence* (NIC) on TURs is usually left unaddressed, with just a couple of notable exceptions (which actually refer to models of quantum absorption refrigerators) [51,68]. We recall that the phenomenon of noise-induced coherence—arising due to interference between different transition paths from the degenerate energy levels to a common level—has been shown to drastically

*varinder@ibs.re.kr

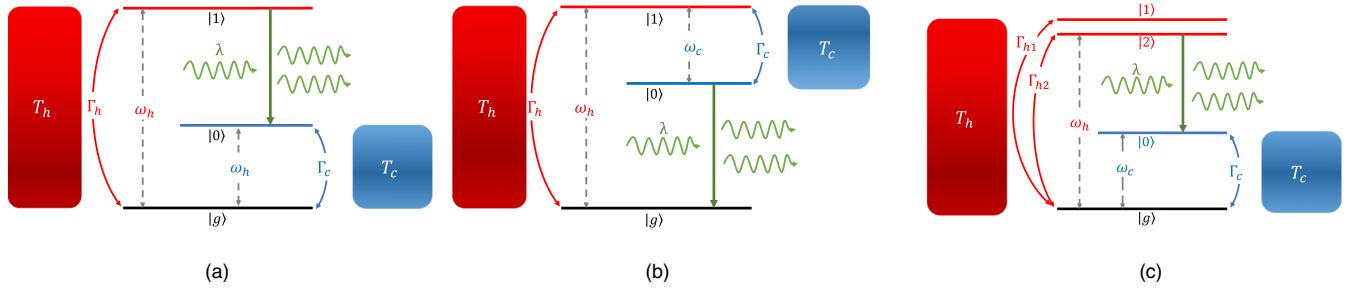


FIG. 1. (a) Model I of the three-level laser heat engine continuously coupled to two reservoirs of temperatures T_h and T_c having coupling constants Γ_h and Γ_c , respectively. The system is interacting with a classical single mode field. λ represents the strength of matter-field coupling. (b) Model II is slightly different from model I. Here, the cold reservoir is connected to two upper levels instead of two lower levels as in model I. Similarly, the power mechanism is coupled to the lower two levels instead of the upper two levels. (c) Four-level degenerate maser heat engine having degeneracy in the upper level.

increase the power output of quantum heat engines [69,70]. Therefore, it is interesting to explore the effects of noise-induced coherence on the power fluctuations in a quantum heat engine.

In this paper, we explore the role of quantum coherence, both drive induced and noise induced, in the violations of the STUR in different variants of maser heat engines, introduced by Scovil and Schulz-Dubois (SSD) back in 1959 [71]. The SSD engine converts the incoherent thermal energy of heat reservoirs into a coherent maser output [71–79] and it is one of the very few experimentally realizable quantum heat engines [80].

Given its prominence—both at the experimental and theoretical level—it is therefore of great interest to curb fluctuations in the power output of the SSD engine, thus motivating a detailed study of the model in the context of TURs. With this motivation in mind, we will first show that the violation of the TUR is *highly* sensitive to the spontaneous emission phenomenon. To reach such a conclusion, we will consider two *slightly* different variants of the three-level SSD model, differing just by the direction of the spontaneous emission term. We will show that such a small difference is sufficient to give very different results when evaluating the TUR quantifier \mathcal{Q} . After this result, we will perform a systematic study of the effect of noise-induced coherence on the violation of the STUR. To this end, we will consider a four-level variant of the SSD model with two degenerate energy levels, and we will compute the STUR quantifier \mathcal{Q} for this model. We will see that the violation of the STUR is *nontrivially* dependent on the specific values taken by the parameters of the model, thus showing the intricacy of the violation patterns and the complex role that noise-induced coherence plays in determining the violation of the STUR.

The paper is organized as follows. In Sec. II we review the SSD model. In Sec. III we study the violations of the STUR for two slightly different variants of the SSD model and compare their respective degrees of violation. In Sec. IV we introduce a variant of the SSD model having two degenerate levels, leading to a scenario suitable to study the effect of noise-induced coherence on violations of the STUR. Such an analysis is then performed in Sec. V. In Sec. VI we conclude our paper.

II. THE SSD MODEL

The SSD engine [71] is one of the most well-known examples of quantum heat engines. In this model, a three-level system is simultaneously coupled to two thermal reservoirs at different temperatures T_c and T_h , with $T_c < T_h$. In a first implementation of the model, that we will call model I [see Fig. 1(a)], the hot reservoir supplies heat to induce a transition between the states $|g\rangle$ and $|1\rangle$, whereas the cold reservoir deexcites the transition between the states $|0\rangle$ and $|g\rangle$. The power output mechanism between states $|0\rangle$ and $|1\rangle$ is modeled by coupling the transition between them to a single-mode classical field. $H_0 = \sum \omega_j |j\rangle\langle j|$ is the free Hamiltonian of the system, where ω_j 's represent the atomic frequencies. The following semiclassical Hamiltonian describes the interaction between the system and the classical field of frequency ω in the rotating wave approximation: $V(t) = \lambda(e^{-i\omega t} |1\rangle\langle 0| + e^{i\omega t} |0\rangle\langle 1|)$; λ is the field-matter coupling constant. When dealing with three-level masers, we will restrict to the case in which the single-mode field is in resonance with the energy gap between the lasing levels $|0\rangle$ and $|1\rangle$, i.e., $\omega = \omega_1 - \omega_0$.

In a reference frame rotating with respect to the system Hamiltonian H_0 , the dynamics of the three-level system is described by the following Lindblad master equation:

$$\dot{\rho} = -i[V_R, \rho] + \mathcal{L}_h[\rho] + \mathcal{L}_c[\rho], \quad (2)$$

where ρ is the density matrix for the three-level system, the coherent part of the dynamics is controlled by $V_R = \lambda(|1\rangle\langle 0| + |0\rangle\langle 1|)$, and $\mathcal{L}_{h(c)}[\rho]$ describes the interaction between the system and the hot (cold) reservoir. In detail, we have

$$\begin{aligned} \mathcal{L}_h[\rho] = & \Gamma_h(n_h + 1)(\sigma_{g1}\rho\sigma_{g1}^\dagger - \frac{1}{2}\{\sigma_{g1}^\dagger\sigma_{g1}, \rho\}) \\ & + \Gamma_h n_h(\sigma_{g1}^\dagger\rho\sigma_{g1} - \frac{1}{2}\{\sigma_{g1}\sigma_{g1}^\dagger, \rho\}), \end{aligned} \quad (3)$$

$$\begin{aligned} \mathcal{L}_c[\rho] = & \Gamma_c(n_c + 1)(\sigma_{g0}\rho\sigma_{g0}^\dagger - \frac{1}{2}\{\sigma_{g0}^\dagger\sigma_{g0}, \rho\}) \\ & + \Gamma_c n_c(\sigma_{g0}^\dagger\rho\sigma_{g0} - \frac{1}{2}\{\sigma_{g0}\sigma_{g0}^\dagger, \rho\}), \end{aligned} \quad (4)$$

where $\sigma_{gk} = |g\rangle\langle k|$ and $k = 0, 1$. Γ_c and Γ_h are system-bath coupling constants for cold and hot reservoirs, respectively. Finally, $n_h = 1/(\exp[\omega_h/T_h] - 1)$ and $n_c = 1/(\exp[\omega_c/T_c] - 1)$ represent the average number of photons with mode

frequencies ω_h and ω_c in the hot and cold reservoirs, respectively ($\omega_c = \omega_0 - \omega_g$, $\omega_h = \omega_1 - \omega_g$).

III. TUR FOR THE SSD MODEL

In this section, we analyze the SSD model from the viewpoint of the TUR and we will compare two slightly different implementations of it. These two implementations differ by which energy levels in the three-level systems are connected by the cold reservoir: in the first implementation, the cold reservoir connects $|g\rangle$ with $|0\rangle$, while in the second the cold reservoir connects $|0\rangle$ with $|1\rangle$. These two configurations are often considered interchangeable in the literature and they

are both referred to as the SSD model [71,72,74–77,80,81]. Despite their similarities, as we will discuss in the following by explicitly studying the TUR, these two configurations give nonequivalent results. We will see that such a difference can be entirely traced to the quantum phenomenon of spontaneous emission and to the nonequivalent role that it plays in the two configurations. The TUR in the first implementation has not been analyzed before while the second implementation is the focus of Refs. [66,67].

A. Model I

First, we will investigate the TUR in model I as shown in Fig. 1(a). The TUR quantifier $\mathcal{Q} = \langle \sigma \rangle \Delta P / \langle P \rangle^2$ is evaluated using the method of full counting statistics; see

Appendix C for details. The calculations yield the following result:

$$\mathcal{Q}^I(\Gamma_h, \Gamma_c, \lambda, n_h, n_c) = \frac{1}{A(n_h - n_c)} \left[A(n_h + n_c + 2n_h n_c) + \frac{8(n_h - n_c)^2 \lambda^2 \Gamma_c \Gamma_h}{A B \Gamma_c \Gamma_h + C \lambda^2} \left(2 - \frac{D + F + G + H}{A B \Gamma_c \Gamma_h + C \lambda^2} \right) \right] \ln \left[\frac{n_h(n_c + 1)}{n_c(n_h + 1)} \right], \quad (5)$$

where $A = \Gamma_c(1 + n_c) + \Gamma_h(1 + n_h)$, $B = 1 + 2n_h + n_c(2 + 3n_h)$, $C = 4[\Gamma_c(1 + 3n_c) + \Gamma_h(1 + 3n_h)]$, $D = (1 + 2n_c)\Gamma_c[(1 + n_c)^2 \Gamma_c^2 + 16\lambda^2]$, $F = (1 + 2n_h)\Gamma_h[(1 + n_h)^2 \Gamma_h^2 + 16\lambda^2]$, $G = (1 + n_c)[7 + 13n_c + 6(2 + 3n_c)]\Gamma_c^2 \Gamma_h$, and $H = (1 + n_h)[7 + 13n_h + 6(2 + 3n_h)]\Gamma_h^2 \Gamma_c$. We note that the first term, $\mathcal{Q}_{\text{pop}} = \ln\{n_h(n_c + 1)/n_c(n_h + 1)\}(n_h + n_c + 2n_h n_c)/(n_h - n_c)$, given in Eq. (5) depends on the bath populations only. Using the inequalities $a/(a - b) \ln(a/b) \geq 1$ and $b/(a - b) \ln(a/b) \geq 1$, we can show that $\mathcal{Q}_{\text{pop}} \geq 2$. Thus we can associate the possible violations of the STUR to negative values of remaining terms in Eq. (5). We also notice that at the verge of the population inversion (threshold condition for the maser) $n_h = n_c$. Thus, we have $\mathcal{Q} = 2$, i.e., the STUR is saturated. Finally, we numerically studied Eq. (5) outside the equilibrium condition and for various values of the parameters. As an example, in Fig. 2 (dashed blue curve) we report Eq. (5) as a function of matter-field coupling strength λ for fixed values of the other parameters. We note a very weak violation of the standard TUR for a certain range of parameter λ . We checked that upon further increasing of λ , \mathcal{Q} gets saturated (not shown). It should be noticed that, no matter how large the value of λ is, the engine can be always taken as working in the weak-coupling regime ($\lambda/\omega \ll 1$). This is because \mathcal{Q}^I , given in Eq. (5), depends on $n_{h,c} = 1/(e^{\omega_{h,c}/T_{h,c}} - 1)$ and not explicitly on $\omega_{h,c}$. Hence, for any given value of $n_{h(c)}$ and by increasing T_h and T_c , we can always choose large enough ω_h and ω_c such that $\omega_h, \omega_c, \omega = \omega_h - \omega_c \gg \lambda$, and thus we always remain in the weak-coupling regime.

It is also interesting to note that, as a consequence of being dimensionless, the TUR quantifier \mathcal{Q} remains invariant if we scale system-bath and matter-field coupling constants by the same factor. In other words, simultaneous transformations of $\Gamma_c \rightarrow k\Gamma_c$, $\Gamma_h \rightarrow k\Gamma_h$, and $\lambda \rightarrow k\lambda$ leave \mathcal{Q} invariant. Mathematically,

$$\mathcal{Q}^I(k\Gamma_h, k\Gamma_c, k\lambda, n_h, n_c) = \mathcal{Q}^I(\Gamma_h, \Gamma_c, \lambda, n_h, n_c). \quad (6)$$

This property allows us to work in units of Γ_c or Γ_h .

Now, we turn our attention to the high-temperature limit. In the high-temperature limit, Eq. (5) can be further simplified. In this regime, we can approximate $n_{h(c)} = T_{h(c)}/\omega_{h(c)} \gg 1$. Then, Eq. (5) reduces to the following form:

$$\mathcal{Q}_{\text{HT}} = 2 - \frac{16(n_h - n_c)^2 \Gamma_h \Gamma_c \lambda^2 (\Gamma_c^2 n_c^2 + \Gamma_h^2 n_h^2 + 5\Gamma_c \Gamma_h n_h n_c + 4\lambda^2)}{9n_h n_c (\Gamma_c n_c + \Gamma_h n_h)^2 (4\lambda^2 + \Gamma_h \Gamma_c n_h n_c)^2}. \quad (7)$$

It is clear from Eq. (7) that, unless $n_h = n_c$, \mathcal{Q}_{HT} is always smaller than 2, which implies that the STUR is always violated in the maser heat engine operating in the high-temperature regime. The STUR violations can be thought of as arising from the coherent quantum dynamics which go

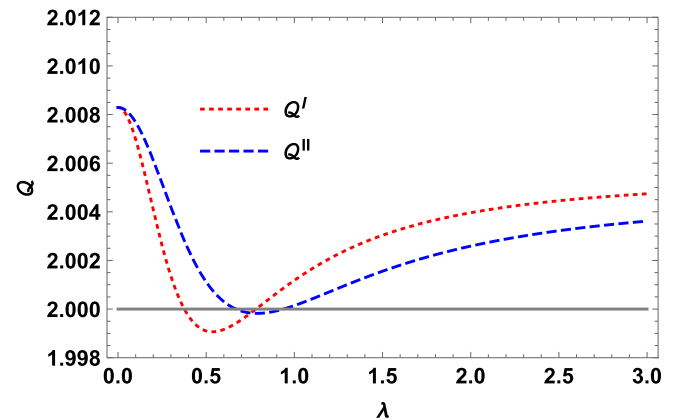


FIG. 2. TUR quantifier \mathcal{Q} vs matter-field coupling parameter λ . Dashed blue and dotted red curves correspond to model I and model II, respectively. Here, we use the invariance of \mathcal{Q} to further set $\Gamma_c = 1$ which, together with the choice $\hbar = k_B = 1$, fully specifies the units used in this plot. We also take $\Gamma_h = 0.1$, $n_h = 5$, $n_c = 2$.

beyond the steady-state coherences as shown in Refs. [66,67]. Though it is usually considered that systems are classical at high temperatures, this is not sufficient per se to claim all the quantum character of the system is vanished. The resolution of the quantum energy levels can be smaller than thermal energy scales at high temperatures so that any spectral distinction of discreteness of the energy becomes impossible. However, there can be still coherence among some energy levels. In the case of a three-level maser engine, this is the case as drive-induced coherence between the energy levels $|0\rangle$ and $|1\rangle$ is always there. As a result, the expression power output of the engine explicitly depends on the coherence between energy levels $|0\rangle$ and $|1\rangle$ and is given by $P = i\lambda(\omega_c - \omega_h)(\rho_{01} - \rho_{10})$ [70,73,76]. In fact, coherence is the necessary ingredient to generate finite-power output in continuous quantum heat engines [74,82]. Further, the STUR violations in the high-temperature limit have already been reported in Refs. [45,60,61].

B. Model II

In this subsection, we consider a slight modification of model I, which we refer to as model II and which is depicted in Fig. 1(b). Certain aspects of TUR violations in this model have already been discussed in Ref. [66]. Here and in the next subsection, we will show that, although the two configurations are very similar (and, as already mentioned previously, they can be seen as the same SSD model for different arrangements of the energy levels), they give quite different results when dealing with violations of the TUR. We will also show that this difference is coming from the spontaneous emission contribution which is not symmetric in the two configurations.

For model II, we have the following expression for the TUR quantifier \mathcal{Q}^{II} :

$$\mathcal{Q}^{\text{II}} = \ln \left[\frac{n_h(n_c + 1)}{n_c(n_h + 1)} \right] \left\{ \frac{n_h + n_c + 2n_h n_c}{n_h - n_c} + \frac{8(n_h - n_c)\Gamma_c \Gamma_h \lambda^2}{A'(A'B' + 4D'\lambda^2)} \left[2 - \frac{A(4B + AC) + 16C\lambda^2}{A'(A'B' + 4D'\lambda^2)} \right] \right\}, \quad (8)$$

where $A' = \Gamma_c n_c + \Gamma_h n_h$, $B' = n_c + n_h + 3n_c n_h$, $C' = \Gamma_c(1 + 2n_c) + \Gamma_h(1 + 2n_h)$, and $D' = \Gamma_c(2 + 3n_c) + \Gamma_h(2 + 3n_h)$. The TUR relation for model II given in Eq. (8) is different from the TUR relation given in Eq. (5) for model I. In Fig. 2, we plot Eq. (8) (dotted red curve) in terms of matter-field coupling constant λ . Also for this model, we see a violation of the STUR for certain values of λ .

C. Comparison between model I and model II

We are now at the position to perform a comparison between the two models just analyzed. As clear from Fig. 2, model II yields a lower TUR ratio for smaller values of λ as compared to model I, whereas for the larger values of λ model II yields better results.

Although both models yield different expressions for the TUR ratio, the first term, $\mathcal{Q}_{\text{pop}} = \ln\{n_h(n_c + 1)/n_c(n_h + 1)\}(n_h + n_c + 2n_h n_c)/(n_h - n_c)$, is the same. \mathcal{Q}_{pop} depends only on the bath populations and is always greater than 2 [66].

Hence, in both models, the second term is responsible for the observed STUR violations. Although STUR violations are not uncommon in our three-level models, still they adhere to the quantum mechanical bound found in Ref. [11], which is two times looser than the STUR. Further, it should be noticed that most of the values of \mathcal{Q}^{I} and \mathcal{Q}^{II} given in Eqs. (5) and (8) lie very close to 2.

In the high-temperature regime, Eq. (8) reduces to Eq. (7). Hence, in the high-temperature limit, both models lead to the same TUR ratio. This can be traced back to the identical dynamical rate equations for both models. In the high-temperature limit, spontaneous emission can be ignored. Therefore the asymmetry between the two models, due to the presence of spontaneous emission, is no longer there. In such a case, model I and model II share a reflection symmetry, thereby yielding identical results. Mathematically, this can be seen as follows. Interchanging the indices $g \rightarrow 1$ in Eqs. (A6)–(A10) and ignoring $\Gamma_{h,c}$ as compared to $\Gamma_{h,c}n_{h,c}$, we obtain the exact same set of equations as given in Eqs. (A1)–(A5). Thus, the contribution coming from spontaneous emission is the only contribution breaking the otherwise symmetry between the two configurations. Hence, we conclude that the two configurations are inequivalent by the presence of the spontaneous emission term only.

To make the comparison between the two models more concrete, we also plot the histograms of sampled values of \mathcal{Q}^{I} and \mathcal{Q}^{II} for random sampling over a region of the parametric space (see Fig. 3). In both cases, for the great majority of sampled operational points, the TUR ratio stays close to the conventional STUR limit $\mathcal{Q} = 2$. This can be explained as follows. As the three-level system is driven by thermal sources, steady-state photon distribution is expected to be close to a thermal state [83], and the second-order coherence function $[g^2(\tau)]$ is equal to 2 for a thermal state, i.e., $g^2(\tau) = 2$ [84,85]. TUR quantifier \mathcal{Q} is, up to some factors, directly expressed in terms of the ratio of the power fluctuations to the square of the mean power. As the radiated power of the atom is given in terms of the photon number operator, such an expression can be written in terms of the zero-time delay second-order coherence function $[g^2(0)]$. Thus, our results suggest that radiated photons in steady state are approximately in thermal states. However, it is clear from the histograms in Fig. 3 that STUR violations are more common in model II. Additionally, as far as the minimum numerical value of the TUR ratio is concerned, model II attains a lower minimum value as compared to model I, i.e., $\mathcal{Q}_{\text{min}}^{\text{II}} < \mathcal{Q}_{\text{min}}^{\text{I}}$.

Summarizing the results of this section, we presented a clear case where the physics of the TUR is highly controlled by the spontaneous emission phenomenon: the two models just differ by the spontaneous emission term and this small difference makes them inequivalent in the way in which they violate the STUR.

IV. A FOUR-LEVEL VERSION OF THE SSD MODEL

In this section, we consider a variant of the SSD model [see Fig. 1(c)], originally introduced in Ref. [69]. In this model, the upper levels $|1\rangle$ and $|2\rangle$ are degenerate. The Hamiltonian of the system in the rotating wave approximation is given by $H_0 = \sum \omega_k |k\rangle \langle k|$ where the summation runs over all four

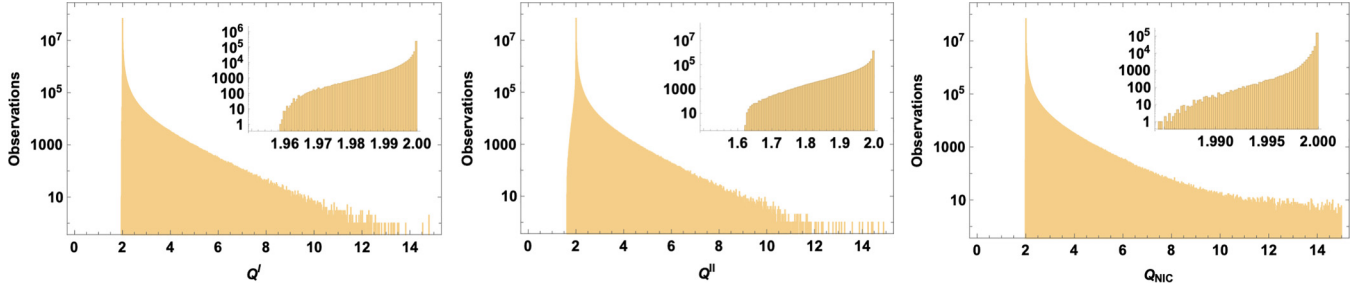


FIG. 3. Histograms of sampled values of Q^I , Q^II , and Q_{NIC} for random sampling over a region of the parametric space. The insets show the subset of the sampled data for which STUR violations are happening. The parameters are sampled over the uniform distributions $\Gamma_{h,c} \in [10^{-4}, 5]$, $n_{h,c} \in [0, 10]$, and $\lambda \in [10^{-4}, 1]$. For plotting the histograms, we choose a bin width of 0.01 to arrange 10^8 data points.

states. The interaction Hamiltonian takes the following form: $V(t) = \lambda e^{-i\omega t} (|1\rangle\langle 0| + |2\rangle\langle 0|) + \text{H.c.}$ The time evolution of the system is described by the following master equation:

$$\dot{\rho} = -i[H_0 + V(t), \rho] + \mathcal{L}_h[\rho] + \mathcal{L}_c[\rho], \quad (9)$$

where $\mathcal{L}_{h(c)}$ represents the dissipative Lindblad superoperator describing the system-bath interaction with the hot (cold) reservoir:

$$\begin{aligned} \mathcal{L}_c[\rho] &= \Gamma_c(n_c + 1) \left(A_c \rho A_c^\dagger - \frac{1}{2} \{A_c^\dagger A_c, \rho\} \right) + \Gamma_c n \left(A_c^\dagger \rho A_c - \frac{1}{2} \{A_c A_c^\dagger, \rho\} \right), \\ \mathcal{L}_h[\rho] &= \sum_{k=1,2} \Gamma_{hk} \left[(n_h + 1) \left(A_k \rho A_k^\dagger - \frac{1}{2} \{A_k^\dagger A_k, \rho\} \right) + n_h \left(A_k^\dagger \rho A_k - \frac{1}{2} \{A_k A_k^\dagger, \rho\} \right) \right] \\ &\quad + \Gamma \cos \theta \left[(n_h + 1) \left(A_1 \rho A_2^\dagger - \frac{1}{2} \{A_2^\dagger A_1, \rho\} \right) + n_h \left(A_1^\dagger \rho A_2 - \frac{1}{2} \{A_2 A_1^\dagger, \rho\} \right) \right] \\ &\quad + \Gamma \cos \theta \left[(n_h + 1) \left(A_2 \rho A_1^\dagger - \frac{1}{2} \{A_1^\dagger A_2, \rho\} \right) + n_h \left(A_2^\dagger \rho A_1 - \frac{1}{2} \{A_1 A_2^\dagger, \rho\} \right) \right] \end{aligned} \quad (10)$$

where $A_c = |g\rangle\langle 0|$ and $A_k = |g\rangle\langle k|$ ($k = 1, 2$) are jump operators between the relevant transitions. θ is the angle between the dipole transitions $|1\rangle \rightarrow |g\rangle$ and $|2\rangle \rightarrow |g\rangle$. $\Gamma = \sqrt{\Gamma_{h1}\Gamma_{h2}}$, where Γ_{h1} and Γ_{h2} are Wigner-Weisskopf constants for transitions between $|g\rangle \rightarrow |1\rangle$ and $|g\rangle \rightarrow |2\rangle$, respectively. To make the discussion analytically traceable, from now on we set $\Gamma_{h1} = \Gamma_{h2} = \Gamma_h$; thus we have $\Gamma = \Gamma_h$.

Physically, the phenomenon of noise-induced coherence arises due to the interference of two indistinguishable decay paths $|1\rangle \rightarrow |g\rangle$ and $|2\rangle \rightarrow |g\rangle$ to the same level $|g\rangle$ [69]. As customary when dealing with noise-induced coherence, we define $p \equiv \cos \theta$ as the noise-induced coherence parameter, lying in the range $(-1, 1)$. For the values of p lying in the range $(p, -1, 0)$, destructive interference takes place between the dipole transitions, whereas in the range $(p, 0, 1)$ dipole transitions interfere constructively.

V. TUR IN THE FOUR-LEVEL DEGENERATE MASER HEAT ENGINE

Having presented the model of a four-level maser heat engine with degenerate upper levels, we are ready to discuss the effects of noise-induced coherence on the thermodynamic uncertainty relation. Noise-induced coherence has been shown to amplify the power of a four-level maser heat engine by a factor of 2 as compared to the three-level nondegenerate model [69,70]. Therefore, it is natural to explore the effects

of noise-induced coherence on relative power fluctuations. In this case, the resulting form of TUR quantifier Q_{NIC} is presented in Eq. (C26) in Appendix C. Equation (C26) is plotted in Fig. 4 as a function of λ for different values of

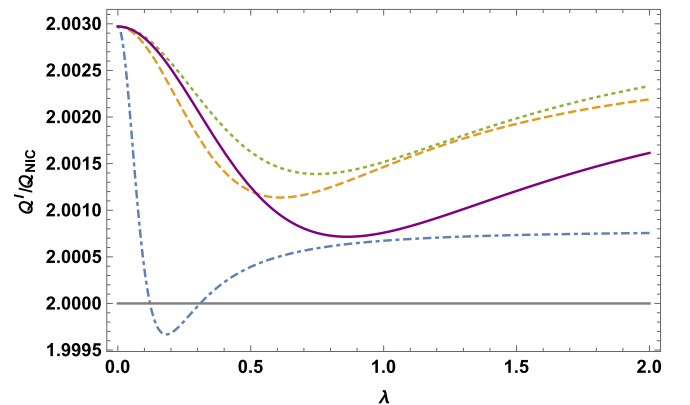


FIG. 4. TUR quantifier Q_{NIC} as a function of λ for different values of noise-induced coherence parameter p . The dot-dashed blue curve, dashed orange curve, and dotted green curve represent the cases for $p = -0.945, 0$, and 0.7 , respectively. The solid violet curve represents the TUR ratio for the three-level engine, model I. Here, we fix units by setting $\Gamma_h = 1$, and we consider the case $\Gamma_c = 0.1$, $n_h = 6$, and $n_c = 3$.

noise-induced coherence parameter p . The solid purple curve in Fig. 4 represents the TUR ratio for the three-level engine, model I. It is clear from Fig. 4 that, depending upon the numeric value of noise-induced coherence parameter p , noise-induced coherence can either suppress or amplify the relative fluctuations in the power output of the degenerate four-level engine as compared to its three-level counterpart. For $p = -0.945$, the dot-dashed violet curve always lies below the solid brown curve for the three-level engine, thereby showing the advantage of noise-induced coherence in suppressing the relative power fluctuations. For $p = 0$, the dashed blue curve representing $Q_{\text{NIC}}(p = 0)$ lies below its three-level counterpart (solid brown curve) for smaller values of λ . However, for relatively higher values of λ , noise-induced coherence is not helpful and amplifies the relative power fluctuations in the engine. For $p = 0.7$, we have a different story altogether. In this case, the dotted red curve (representing the case $p = 0.7$) always lies above the solid brown curve (for a three-level engine), which implies that noise-induced coherence amplifies the power relative fluctuations in the engine for the entire range of λ . Thus, we can conclude that, depending on the parametric operation regime, the noise-induced coherence phenomenon can either suppress or amplify the relative power fluctuations in a degenerate maser heat engine compared to its nondegenerate counterpart. This is in contrast to the earlier studies in which noise-induced coherence has been shown to have only detrimental effects on the TUR in quantum absorption refrigerators [51,68]. In both the above-mentioned studies, the STUR is always satisfied in the presence of noise-induced coherence. The main message of our paper is that, by fine tuning the system-bath parameters involved in the study of the degenerate maser heat engine (or choosing the proper parametric regime), noise-induced coherence can be used to suppress relative power fluctuations along with amplifying the power of the engine at the same time [69,70]. In conclusion, noise-induced coherence can be treated as a quantum resource in enhancing the performance of quantum heat engines and it is free of cost, unlike drive-induced coherence.

To make our analysis more complete, we also study the case when the driving field is not at resonance with the energy gap between the levels $|0\rangle$ and $|1(2)\rangle$. By fixing all other parameters, we plot TUR quantifier Q_{NIC} given in Eq. (C26) as a function of detuning parameter Δ [$\Delta = \omega - (\omega_1 - \omega_0)$] in Fig. 5. The effect of detuning Δ on the TUR in the degenerate four-level maser heat engine is the same as that for the nondegenerate three-level engine [66]. When plotted against the detuning parameter Δ , Q_{NIC} is minimum for $\Delta = 0$, and symmetric around the point $\Delta = 0$.

Having discussed the behavior of Q_{NIC} as a function of matter-field coupling parameter λ , we move to discuss the behavior of Q_{NIC} as a function of noise-induced coherence parameter p with all other parameters kept fixed at constant values. It is evident from Fig. 6 that Q_{NIC} exhibits a minimum at a certain numerical value of p lying in the range $[-1, 1]$. We note that, for $p = -1$, Q_{NIC} is always greater than 2 regardless of the choice of all system-bath parameters. This can be seen analytically. For $p = -1$, we derive following form of TUR

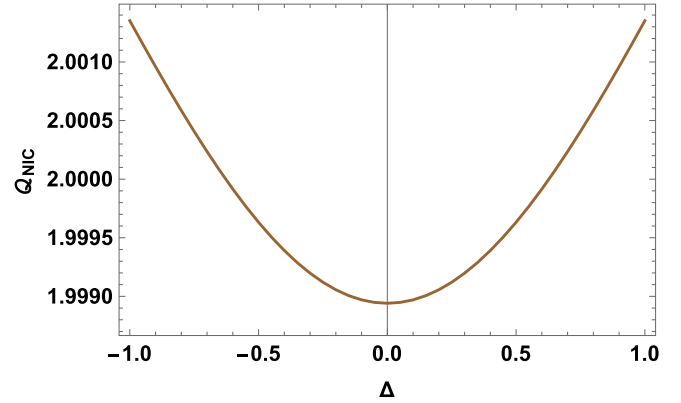


FIG. 5. Q_{NIC} as a function of detuning parameter Δ [$\Delta = \omega - (\omega_1 - \omega_0)$]. Here, $\Gamma_h = 1$, $\Gamma_c = 0.5$, $p = -0.97$, $\lambda = 0.7$, $n_h = 40$, and $n_c = 3$.

quantifier Q_{NIC} :

$$Q_{\text{NIC}}(p = -1) = \ln \left[\frac{n_h(n_c + 1)}{n_c(n_h + 1)} \right] \frac{n_h + n_c + 2n_h n_c}{n_h - n_c}, \quad (12)$$

which is nothing but the already introduced term Q_{pop} . We have already shown in Sec. III that $Q_{\text{pop}} \geq 2$.

In the high-temperature limit, we have an interesting result. In this case, we can show that Q_{NIC} is always equal to 2 regardless of the choice of other system-bath parameters:

$$Q_{\text{NIC}}^{\text{HT}} = 2. \quad (13)$$

This is in contrast to the case with the three-level engine. In that case, the TUR ratio Q_{HT} is always less than 2 unless $n_h = n_c$. It implies that in the high-temperature regime the phenomenon of noise-induced coherence always amplifies the relative power fluctuations.

One more comment is in order here. As clear from Fig. 6, the Q_{NIC} diverges for $p = 1$. As mean power output is finite

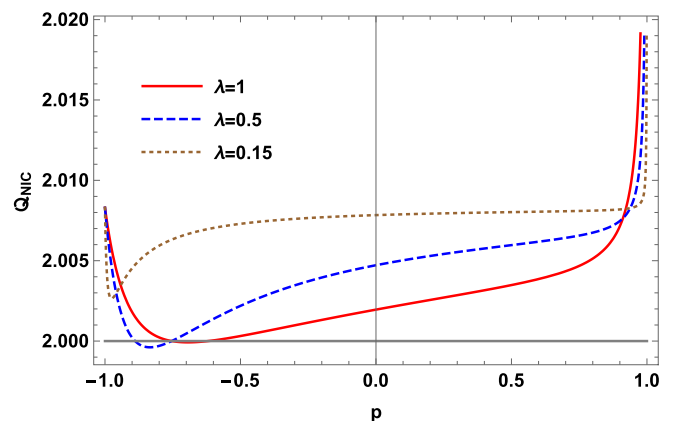


FIG. 6. Q_{NIC} as a function of noise-induced coherence parameter p for different values of λ . Solid red, dashed blue, and dotted brown curves represent the cases for $\lambda = 1$, $\lambda = 0.5$, and $\lambda = 0.15$, respectively. Here, $\Gamma_h = 1$, $\Gamma_c = 0.5$, $n_h = 5$, and $n_c = 2$.

at $p = 1$, this implies that power fluctuations (scale variance of power) diverge at $p = 1$. This is an important point, as in Refs. [69,70] it was shown that the power of the engine can be doubled for $p = 1$. However, our result shows that it is not a good idea to operate a maser heat engine exactly at $p = 1$ but rather at a lower value of p .

Finally, we plot the histogram of sampled values of \mathcal{Q}_{NIC} for random sampling over a region of the parametric space [see Fig. 3(c)]. Similar to the three-level case, for the great majority of sampled operational points, the TUR ratio stays close to 2. However, the minimum value of \mathcal{Q}_{NIC} extracted from the histogram [see inset of Fig. 3(c)] is 1.985, which is greater than the corresponding case of the three-level engine (model I), i.e., $\mathcal{Q}_{\text{min}}^{\text{I}} < \mathcal{Q}_{\text{NIC}}^{\text{II}}$.

VI. CONCLUSIONS

We have presented a detailed analysis of thermodynamic uncertainty relations in nondegenerate three-level and degenerate four-level maser heat engines. For the nondegenerate three-level maser heat engine, we studied two slightly different configurations of the engine and obtained analytical expressions for the TUR ratio. We have shown that, although very similar, the two configurations have very different violation patterns of STUR, and they agree in the high-temperature regime only. We used this result to uncover the very subtle and nontrivial role that spontaneous emission plays in determining the violation of the STUR. Further, for the degenerate four-level engine, we studied the effects of noise-induced coherence on the TUR. We showed that, depending on the parametric regime of operation, the phenomenon of noise-induced coherence can either suppress or amplify the relative power fluctuations. In this way, we have shown also the intricacy of the role that noise-induced coherence plays in determining the violation of the STUR.

As noted in Sec. III, the violation of the STUR might be traced back to contributions (sometimes positive, sometimes negative) coming from coherence. Hence, it would be very interesting to calculate the exact contribution of coherences in the violation of the standard TUR. To this end, it is necessary to go beyond the steady state and use the quantum trajectory approach to unravel the master equation [67]. We hope to address this point in the near future.

ACKNOWLEDGMENTS

Varinder Singh, Vahid Shaghghi, and D.R. acknowledge support from the Institute for Basic Science in Korea (Grant No. IBS-R024-D1). We thank Matteo Carrega and Jae Sung Lee for interesting discussions.

APPENDIX A: DENSITY-MATRIX EQUATIONS FOR THREE-LEVEL MASER HEAT ENGINE

Here, we will present the density-matrix equations for the two different variants of the SSD engine.

1. Model I

For the three-level system shown in Fig. 1(a), the time evolution of the elements of the density matrix is governed by the following equations [70,73,76]:

$$\dot{\rho}_{gg} = \Gamma_h(n_h + 1)\rho_{11} + \Gamma_c(n_c + 1)\rho_{00} - (\Gamma_h n_h + \Gamma_c n_c)\rho_{gg}, \quad (\text{A1})$$

$$\dot{\rho}_{11} = i\lambda(\rho_{10} - \rho_{01}) - \Gamma_h[(n_h + 1)\rho_{11} - n_h\rho_{gg}], \quad (\text{A2})$$

$$\dot{\rho}_{00} = -i\lambda(\rho_{10} - \rho_{01}) - \Gamma_c[(n_c + 1)\rho_{00} - n_c\rho_{gg}], \quad (\text{A3})$$

$$\dot{\rho}_{10} = i\lambda(\rho_{11} - \rho_{00}) - \frac{1}{2}[\Gamma_h(n_h + 1) + \Gamma_c(n_c + 1)]\rho_{10}, \quad (\text{A4})$$

$$\dot{\rho}_{01} = \dot{\rho}_{10}^*. \quad (\text{A5})$$

2. Model II

For the three-level system shown in Fig. 1(b), the dynamical equations for different density-matrix elements are given by

$$\dot{\rho}_{11} = \Gamma_h n_h \rho_{gg} + \Gamma_c n_c \rho_{00} - [\Gamma_h(n_h + 1) + \Gamma_c(n_c + 1)]\rho_{11}, \quad (\text{A6})$$

$$\dot{\rho}_{00} = \Gamma_c(n_c + 1)\rho_{11} - \Gamma_c n_c \rho_{00} + i\lambda(\rho_{g0} - \rho_{g0}), \quad (\text{A7})$$

$$\dot{\rho}_{gg} = \Gamma_h(n_h + 1)\rho_{11} - \Gamma_h n_h \rho_{gg} - i\lambda(\rho_{g0} - \rho_{g0}), \quad (\text{A8})$$

$$\dot{\rho}_{g0} = i\lambda(\rho_{00} - \rho_{gg}) - \frac{1}{2}(\Gamma_h n_h + \Gamma_c n_c)\rho_{g0}, \quad (\text{A9})$$

$$\dot{\rho}_{0g} = \dot{\rho}_{g0}^*. \quad (\text{A10})$$

Notice that, by interchanging the indices $g \rightarrow 1$ in Eqs. (A6)–(A10) and ignoring $\Gamma_{h,c}$ as compared to $\Gamma_{h,c} n_{h,c}$, i.e., the term related to spontaneous emission, we obtain the exact same set of equations as given in Eqs. (A1)–(A5).

APPENDIX B: MASTER EQUATION FOR THE FOUR-LEVEL MASER HEAT ENGINE

Consider a modified version of the SSD engine where we have replaced a single upper level $|1\rangle$ by a pair of two degenerate states $|1\rangle$ and $|2\rangle$. Then the bare Hamiltonian of the four-level system and the semiclassical system-field interaction Hamiltonian are given by [70]

$$H_0 = \sum_{i=g,0,1,2} \omega_i |i\rangle \langle i|, \quad (\text{B1})$$

$$V(t) = \lambda[e^{-i\omega t} (|1\rangle \langle 0| + |2\rangle \langle 0|) + e^{i\omega t} (|0\rangle \langle 1| + |0\rangle \langle 2|)]. \quad (\text{B2})$$

In a rotating frame with respect to H_0 , the time evolution of the system is described by the following master equation:

$$\dot{\rho} = -i[H_0 + V(t), \rho] + \mathcal{L}_h[\rho] + \mathcal{L}_c[\rho], \quad (\text{B3})$$

where $\mathcal{L}_{h(c)}$ represents the dissipative Lindblad superoperator describing the system-bath interaction with the hot

(cold) reservoir, Eqs. (10) and (11), that we repeat here for convenience:

$$\mathcal{L}_c[\rho] = \Gamma_c(n_c + 1) \left(A_c \rho A_c^\dagger - \frac{1}{2} \{A_c^\dagger A_c, \rho\} \right) + \Gamma_c n_c \left(A_c^\dagger \rho A_c - \frac{1}{2} \{A_c A_c^\dagger, \rho\} \right), \quad (\text{B4})$$

$$\begin{aligned} \mathcal{L}_h[\rho] = & \sum_{k=1,2} \Gamma_{hk} \left[(n_h + 1) \left(A_k \rho A_k^\dagger - \frac{1}{2} \{A_k^\dagger A_k, \rho\} \right) + n_h \left(A_k^\dagger \rho A_k - \frac{1}{2} \{A_k A_k^\dagger, \rho\} \right) \right] \\ & + \Gamma \cos \theta \left[(n_h + 1) \left(A_1 \rho A_2^\dagger - \frac{1}{2} \{A_2^\dagger A_1, \rho\} \right) + n_h \left(A_1^\dagger \rho A_2 - \frac{1}{2} \{A_2 A_1^\dagger, \rho\} \right) \right] \\ & + \Gamma \cos \theta \left[(n_h + 1) \left(A_2 \rho A_1^\dagger - \frac{1}{2} \{A_1^\dagger A_2, \rho\} \right) + n_h \left(A_2^\dagger \rho A_1 - \frac{1}{2} \{A_1 A_2^\dagger, \rho\} \right) \right] \end{aligned} \quad (\text{B5})$$

where $A_c = |g\rangle\langle 0|$ and $A_k = |g\rangle\langle k|$ ($k = 1, 2$) are jump operators between the relevant transitions. The time evolution of the density-matrix equations is given by

$$\dot{\rho}_{11} = i\lambda(\rho_{10} - \rho_{01}) - \Gamma_h[(n_h + 1)\rho_{11} - n_h\rho_{gg}] - \frac{1}{2}p\Gamma_h(n_h + 1)(\rho_{12} + \rho_{21}), \quad (\text{B6})$$

$$\dot{\rho}_{22} = i\lambda(\rho_{20} - \rho_{02}) - \Gamma_h[(n_h + 1)\rho_{22} - n_h\rho_{gg}] - \frac{1}{2}p\Gamma_h(n_h + 1)(\rho_{12} + \rho_{21}), \quad (\text{B7})$$

$$\begin{aligned} \dot{\rho}_{00} &= i\lambda(\rho_{01} + \rho_{02} - \rho_{10} - \rho_{20}) - \Gamma_c[(n_c + 1)\rho_{00} - n_c\rho_{gg}], \\ \rho_{gg} &= 1 - \rho_{11} - \rho_{22} - \rho_{00}, \end{aligned} \quad (\text{B8})$$

$$\dot{\rho}_{12} = i\lambda(\rho_{10} - \rho_{02}) - \frac{1}{2}[\Gamma_h(n_h + 1) + \Gamma_h(n_h + 1)]\rho_{12} - \frac{1}{2}p\Gamma_h[(n_h + 1)\rho_{11} + (n_h + 1)\rho_{22} - (n_h + n_h)\rho_{gg}], \quad (\text{B9})$$

$$\dot{\rho}_{10} = i\lambda(\rho_{11} - \rho_{00} + \rho_{12}) - \frac{1}{2}[\Gamma_c(n_c + 1) + \Gamma_h(n_h + 1)]\rho_{10} - \frac{1}{2}p\Gamma_h(n_h + 1)\rho_{20}, \quad (\text{B10})$$

$$\dot{\rho}_{20} = i\lambda(\rho_{22} - \rho_{00} + \rho_{21}) - \frac{1}{2}[\Gamma_c(n_c + 1) + \Gamma_h(n_h + 1)]\rho_{20} - \frac{1}{2}p\Gamma_h(n_h + 1)\rho_{10}. \quad (\text{B11})$$

APPENDIX C: FULL COUNTING STATISTICS

In order to calculate \mathcal{Q} , we first need to calculate the mean and the variance of the power along with the rate of entropy production. For the steady-state heat engines obeying the strong-coupling condition (no heat leaks between the reservoirs), the relation between the energy flux (heat and work fluxes) I_E and matter flux (here photon flux) $\langle I \rangle$ ($\langle I \rangle > 0$) is given by [86]

$$\langle I_E \rangle = \epsilon \langle I \rangle. \quad (\text{C1})$$

The above equation implies that the energy is transported by the particles of a given energy ϵ . Here, we have applied the tight-coupling condition on the average currents. Such a coupling can be achieved in nanoscale devices [87–91] and masers [86]. In maser heat engines, the tight-coupling condition is naturally obeyed as energy from the reservoirs to the system is transported at a single frequency. The heat flux entering into the system from the hot reservoir carries photons of frequency ω_h only and the heat flux dumped into the cold reservoir contains photons of frequency ω_c only.

In this paper, we are using a sign convention in which all the incoming fluxes entering (leaving) into (out of) the three-level system are taken to be positive (negative). Applying the first law of thermodynamics, we have $\langle P \rangle + \langle \dot{Q}_h \rangle + \langle \dot{Q}_c \rangle = 0$. For heat engines, $\langle \dot{Q}_h \rangle > 0$, $\langle \dot{Q}_c \rangle < 0$, and $\langle P \rangle < 0$. Applying the tight-coupling condition to the heat fluxes and then using

the relation $\langle P \rangle = -(\langle \dot{Q}_h \rangle + \langle \dot{Q}_c \rangle)$, we have

$$\langle \dot{Q}_h \rangle = \omega_h \langle I \rangle, \quad \langle \dot{Q}_c \rangle = -\omega_c \langle I \rangle, \quad \langle P \rangle = (\omega_c - \omega_h) \langle I \rangle. \quad (\text{C2})$$

Since all the fluxes are proportional to each other, the TUR will be exactly the same for all currents. Similarly, the variance of the power is given by $\text{var}(P) = (\omega_h - \omega_c)^2 \text{var}(I)$. Using these relations, the TUR ratio \mathcal{Q} can be written as

$$\mathcal{Q} = \langle \sigma \rangle \frac{\Delta P}{\langle P \rangle^2} = \langle \sigma \rangle \frac{\Delta I}{\langle I \rangle^2}. \quad (\text{C3})$$

Further, the average rate of entropy production is given by

$$\langle \sigma \rangle = -\frac{\dot{Q}_c}{T_c} - \frac{\dot{Q}_h}{T_h}. \quad (\text{C4})$$

By using the relations $n_h = 1/(e^{\omega_h/T_h} - 1)$ and $n_c = 1/(e^{\omega_c/T_c} - 1)$, the temperatures of the reservoirs can be expressed in terms of the average number of photons n_h and n_c as follows:

$$\frac{1}{T_h} = \frac{1}{\omega_h} \ln \left[\frac{n_h + 1}{n_h} \right], \quad \frac{1}{T_c} = \frac{1}{\omega_c} \ln \left[\frac{n_c + 1}{n_c} \right]. \quad (\text{C5})$$

Combining Eqs. (C2), (C4), and (C5), after a little algebra we obtain

$$\langle \sigma \rangle = \ln \left[\frac{n_h(n_c + 1)}{n_c(n_h + 1)} \right] \langle I \rangle > 0. \quad (\text{C6})$$

Further, using Eq. (C6) in Eq. (C3), we have

$$\mathcal{Q} = \ln \left[\frac{n_h(n_c + 1)}{n_c(n_h + 1)} \right] \frac{\Delta I}{\langle I \rangle}. \quad (\text{C7})$$

Now we will evaluate the expression for the photon flux $\langle I \rangle$. In open quantum systems, particle statistics can be determined by using the formalism of full counting statistics, where counting fields are incorporated in the master equation. For our purpose, it is sufficient to introduce a counting field for either the hot or the cold reservoir. Here, we choose to introduce the counting field (χ) for the cold reservoir [92,93]. The modified Lindblad master equation takes the following

$$\mathcal{L}(\chi) = \begin{bmatrix} -(\Gamma_h n_h + \Gamma_c n_c) & \Gamma_c(n_c + 1)e^{-i\chi} & \Gamma_h(n_h + 1) & 0 & 0 \\ \Gamma_c n_c e^{i\chi} & -\Gamma_c(n_c + 1) & 0 & -i\lambda & i\lambda \\ \Gamma_h n_h & 0 & -\Gamma_h(n_h + 1) & i\lambda & -i\lambda \\ 0 & -i\lambda & i\lambda & 0 & 0 \\ 0 & i\lambda & -i\lambda & 0 & 0 \end{bmatrix} - \frac{1}{2} [\Gamma_h(n_h + 1) + \Gamma_c(n_c + 1)] \begin{bmatrix} 0 & 0 \\ -i\lambda & i\lambda \\ i\lambda & -i\lambda \\ 0 & 0 \\ 0 & -\frac{1}{2} [\Gamma_h(n_h + 1) + \Gamma_c(n_c + 1)] \end{bmatrix}. \quad (\text{C11})$$

For $\chi \rightarrow 0$, Eq. (C11) reduces to the original Liouvillian operator [given in Eq. (4)] for standard time evolution.

In the long-time limit, the k th cumulant of the integrated number of quanta (number of photons here) emitted into the cold reservoir can be determined by [93]

$$C^k(t) = (i\partial_\chi)^k [\xi(\chi)t]_{\chi=0} \equiv (i\partial_\chi)^k \lambda'(t)|_{\chi=0}, \quad (\text{C12})$$

where $\xi(\chi)$ is the eigenvalue of $\mathcal{L}(\chi)$ with the largest real part and $\lambda'(t) = \xi(\chi)t$ in Eq. (C12) is the cumulant generating function for the integrated current (total charge). In order to get the cumulants for the average current in the long-time limit, we define the following scaled cumulant generating function [12,93]:

$$\lambda'_{\text{scaled}} = \lim_{t \rightarrow \infty} \frac{\lambda'(t)}{t} = \xi(\chi). \quad (\text{C13})$$

The first cumulant of λ'_{scaled} corresponds to the mean current $\langle I \rangle$ and the second cumulant corresponds to the *scaled* variance $\Delta I = \lim_{t \rightarrow \infty} \langle [I(t) - \langle I \rangle]^2 \rangle t$:

$$\langle I \rangle \simeq i\partial_\chi \xi(\chi)|_{\chi=0}, \quad \Delta I \simeq -\partial_\chi^2 \xi(\chi)|_{\chi=0}. \quad (\text{C14})$$

To obtain the expressions for the mean and variance, we follow the method explained in Ref. [92]. Consider the characteristic polynomial of $\mathcal{L}(\chi)$:

$$\sum_n c_n \xi^n = 0, \quad (\text{C15})$$

where the terms c_n are functions of χ . Define

$$c'_n = i\partial_\chi c_n|_{\chi=0}, \quad c''_n = (i\partial_\chi)^2 c_n|_{\chi=0} = -\partial_{\chi_n}^2 c_n|_{\chi=0}. \quad (\text{C16})$$

form:

$$\dot{\rho} = -i[V_R, \rho] + \mathcal{L}_h[\rho] + \mathcal{L}_c^\chi[\rho], \quad (\text{C8})$$

where the modified Lindblad superoperator

$$\mathcal{L}_c[\rho] = \Gamma_c(n_c + 1)(e^{-i\chi} \sigma_{g0} \rho \sigma_{g0}^\dagger - \frac{1}{2} \{\sigma_{g0}^\dagger \sigma_{g0}, \rho\}) + \Gamma_c n_c (e^{i\chi} \sigma_{g0}^\dagger \rho \sigma_{g0} - \frac{1}{2} \{\sigma_{g0} \sigma_{g0}^\dagger, \rho\}). \quad (\text{C9})$$

By vectorizing the density-matrix elements into a state vector $\rho_R = (\rho_{gg}, \rho_{00}, \rho_{11}, \rho_{10}, \rho_{01})^T$, we can write the above Lindblad master equation as a matrix equation with the Liouvillian supermatrix $\mathbf{L}(\chi)$:

$$\dot{\rho} = \mathbf{L}(\chi)\rho, \quad (\text{C10})$$

where

$$\mathbf{L}(\chi) = \begin{bmatrix} 0 & 0 \\ -i\lambda & i\lambda \\ i\lambda & -i\lambda \\ -\frac{1}{2} [\Gamma_h(n_h + 1) + \Gamma_c(n_c + 1)] & 0 \\ 0 & -\frac{1}{2} [\Gamma_h(n_h + 1) + \Gamma_c(n_c + 1)] \end{bmatrix}. \quad (\text{C11})$$

Differentiating Eq. (C15) with respect to the counting parameter χ , and then evaluating the resulting equation at $\chi = 0$, we have

$$\left[i\partial_\chi \sum_n c_n \xi^n \right]_{\chi=0} = \sum_n [c'_n + (n+1)c_{n+1}\xi'] \xi^n(0) = 0. \quad (\text{C17})$$

By taking the second-order derivative of Eq. (C15), we find

$$\left[(i\partial_\chi)^2 \sum_n c_n \xi^n \right]_{\chi=0} = \sum_n [c''_n + 2(n+1)c'_{n+1}\xi' + (n+1)c_{n+1}\xi'' + (n+1)(n+2)c_{n+2}\xi'^2] \xi^n(0) = 0. \quad (\text{C18})$$

As the zeroth term $\xi^0 = 1$ should vanish, hence Eq. (C17) implies

$$c'_0 + c_1 \xi' = 0, \quad (\text{C19})$$

from which we obtain the expression for the current:

$$\langle I \rangle = \xi' = -\frac{c'_0}{c_1}. \quad (\text{C20})$$

Similarly, from Eq. (C18), we obtain the following expression for the variance:

$$\Delta I = \xi'' = -\frac{c''_0 + 2I(c'_1 + c_2 I)}{c_1} = 2 \frac{c'_0 c_1 c'_1 - c_0'^2 c_1}{c_1^3} - \frac{c''_0}{c_1}. \quad (\text{C21})$$

Applying the above-mentioned procedure to the Liouvillian given in Eq. (C11), we obtain

$$\begin{aligned}
c'_0 &= (n_h - n_c)\Gamma_h\Gamma_c\Gamma'\lambda^2, \\
c''_0 &= (2n_h n_c + n_h + n_c)\Gamma_h\Gamma_c\Gamma'\lambda^2, \\
c_1 &= \frac{1}{4}\Gamma'\{(3n_h n_c + 2n_h + 2n_c + 1)\Gamma_c\Gamma_h\Gamma' + 4[\Gamma_h(3n_h + 1) + \Gamma_c(3n_c + 1)]\lambda^2\}, \\
c'_1 &= 2(n_h - n_c)\Gamma_h\Gamma_c\lambda^2, \\
c_2 &= -\frac{1}{4}\{(n_h + 1)^2(2n_h + 1)\Gamma_h^3 + (n_c + 1)^2(2n_c + 1)\Gamma_c^3 + (n_h + 1)[7 + 13n_h + 6(2 + 3n_h)n_c] \\
&\quad + (n_c + 1)[7 + 13n_c + 6(2 + 3n_c)n_h]\} - 4[(2n_h + 1)\Gamma_h + (2n_c + 1)\Gamma_c]
\end{aligned} \tag{C22}$$

where $\Gamma' = \Gamma_h(n_h + 1) + \Gamma_c(n_c + 1)$. This provides the current:

$$\langle I \rangle = \frac{4(n_h - n_c)\Gamma_h\Gamma_c\lambda^2}{4\lambda^2[\Gamma_h(3n_h + 1) + \Gamma_c(3n_c + 1)] + (3n_h n_c + 2n_h + 2n_c + 1)[\Gamma_h(n_h + 1) + \Gamma_c(n_c + 1)]\Gamma_h\Gamma_c}. \tag{C23}$$

In a similar manner, using Eq. (C21) we can obtain the expression for $\text{var}(I)$, and further using this expression in Eq. (C7) we finally obtain the expression for TUR ratio \mathcal{Q}^I as given by Eq. (5) in the main text.

By repeating the steps from Eqs. (C8)–(C21) with $V_R = \lambda(|1\rangle\langle 0| + |2\rangle\langle 0| + |0\rangle\langle 1| + |0\rangle\langle 2|)$ and $\mathcal{L}_h[\rho]$ [given in Eq. (B5)], we can obtain the expressions for power $\langle P \rangle_{\text{NIC}}$ and TUR ratio \mathcal{Q}_{NIC} of the four-level maser heat engine as given below (see Supplemental Material [94] for details):

$$\begin{aligned}
\langle P \rangle_{\text{NIC}} &= 8\lambda^2(p + 1)\Gamma_c\Gamma_h(\omega_c - \omega_h)(n_h + 1)(n_h - n_c) / \{(p + 1)(n_c + 1)(n_h + 1) + 8\lambda^2(p + 1)\Gamma_h(n_h + 1) \\
&\quad \times (4n_h + 1)\Gamma_c^2\Gamma_h[n_c(4n_h + 2) + 3n_h + 1] + \Gamma_c[8\lambda^2(4n_c n_h + 3n_c + 2n_h + 1) + (p + 1)^2\Gamma_h^2(n_h + 1)^2 \\
&\quad \times (4n_c n_h + 2n_c + 3n_h + 1)]\},
\end{aligned} \tag{C24}$$

$$\begin{aligned}
\mathcal{Q}_{\text{NIC}} &= \ln \left[\frac{n_h(n_c + 1)}{n_c(n_h + 1)} \right] \{ 4(p - 1)(p + 1)^2 n_c^5 (n_h + 1)^2 (2n_h + 1)^3 \Gamma_h^2 \Gamma_c^4 + 4(p + 1) n_c^4 (n_h + 1) \Gamma_h \Gamma_c^3 (32\lambda^2 \{ n_h [4(p - 1)n_h \\
&\quad + (4n_h + 7) + 14p - 15] + 2(p - 1)\} + (p - 1)(p + 1)\Gamma_c\Gamma_h(n_h + 1)(8n_h + 3)(2n_h + 1)^2 + 2(p - 1)(p + 1)^2 \\
&\quad \times \Gamma_h^2(n_h + 1)^2(2n_h + 1)^3) + n_c^3 \Gamma_c^2 [(p - 1)(p + 1)^2 \Gamma_c^2 \Gamma_h^2(n_h + 1)^2(2n_h + 1)[n_h(101n_h + 74) + 13] + 16(p + 1)\Gamma_c \\
&\quad \times \Gamma_h(n_h + 1)[8\lambda^2(n_h\{n_h[44(p - 1)n_h + 73p - 71] + 33p - 35\} + 4(p - 1)) + (p - 1)(p + 1)^2 \Gamma_h^2(n_h + 1)^2(2n_h + 1)^2 \\
&\quad \times (3n_h + 1)] + 4(256\lambda^4\{4n_h[8(p - 1)n_h(n_h + 2) + 10p - 11] + 9(p - 1)\} + 16\lambda^2(p + 1)^2(n_h + 1)^2 \\
&\quad \times \Gamma_h^2(n_h(32(p - 1)n_h(2n_h + 3) + 33p - 35) + p - 1) + (p - 1)(p + 1)^4 \Gamma_h^4(n_h + 1)^4(2n_h + 1)^3) \\
&\quad + n_h[(p - 1)(p + 1)^2 \Gamma_c^4 \Gamma_h^2(n_h + 1)^2(3n_h + 1)^2 + 1024\lambda^4(p - 1)(p + 1)^2 \Gamma_h^2(n_h + 1)^2(4n_h + 1)^2 + 64(p + 1) \\
&\quad \times \lambda^2 \Gamma_c \Gamma_h(n_h + 1)((p - 1)(p + 1)^2 \Gamma_h^2(n_h + 1)^2(3n_h + 1)^2 + 32\lambda^2(n_h(3pn_h - 5n_h + 4p - 4) + p - 1)) \\
&\quad + 2(p + 1)\Gamma_c^3 \Gamma_h(n_h + 1)((p - 1)(p + 1)^2 \Gamma_h^2(n_h + 1)^2(3n_h + 1)^2 + 32\lambda^2(n_h(3pn_h - 5n_h + 4p - 4) + p - 1)) \\
&\quad + \Gamma_c^2(128\lambda^2(p + 1)^2 \Gamma_h^2(n_h + 1)^2(n_h(3pn_h - 4n_h + 4p - 4) + p - 1) + (p - 1)(p + 1)^4 \Gamma_h^4(n_h + 1)^4(3n_h + 1)^2 \\
&\quad + 1024\lambda^4(2n_h(p(n_h + 2) - 3n_h - 2) + p - 1)] \\
&\quad + n_c^2 \Gamma_c \{ (p - 1)(p + 1)^2 \Gamma_c^3 \Gamma_h^2(n_h + 1)^2(n_h(n_h(157n_h + 168) + 57) + 6) + 2(p + 1)\Gamma_c^2 \Gamma_h(n_h + 1) \\
&\quad \times [32\lambda^2(p(n_h + 1)(7n_h + 1)(12n_h + 5) - 86n_h^3 - 123n_h^2 - 54n_h - 5) + (p - 1)(p + 1)^2(n_h + 1)^2 \\
&\quad \times \Gamma_h^2(2n_h + 1)(n_h(53n_h + 34) + 5)] + 64\lambda^2(p + 1)\Gamma_h(n_h + 1) \\
&\quad \times (32\lambda^2(n_h(16(p - 1)n_h(2n_h + 3) + 17p - 19) + p - 1) + (p - 1)(p + 1)^2 \Gamma_h^2(n_h + 1)^2(n_h(8n_h(4n_h + 5) + 13) + 1)) \\
&\quad + 4\Gamma_c\{256\lambda^4[n_h(4n_h(12(p - 1)n_h + 21p - 19) + 39p - 43) + 6(p - 1)] + 32\lambda^2(p + 1)^2(n_h + 1)^2 \\
&\quad \times \Gamma_h^2(n_h[n_h(64(p - 1)n_h + 95p - 93) + 33p - 34] + 2(p - 1)) + (p - 1)(p + 1)^4 \Gamma_h^4(n_h + 1)^4(2n_h + 1)^2(4n_h + 1)\} \\
&\quad + n_c[1024\lambda^4(p - 1)(p + 1)^2 \Gamma_h^2(n_h + 1)^2(2n_h + 1)(4n_h + 1)^2 + (p - 1)(p + 1)^2 \Gamma_c^4 \Gamma_h^2(n_h + 1)^2(3n_h + 1) \\
&\quad \times (n_h(20n_h + 11) + 1) \\
&\quad + 2(p + 1)\Gamma_c^3 \Gamma_h(n_h + 1)[32\lambda^2[n_h(n_h(31pn_h - 35n_h + 45p - 41) + 15(p - 1)) + p - 1] + (p - 1)(p + 1)^2 \Gamma_h^2 \\
&\quad \times (n_h + 1)^2(3n_h + 1)(n_h(17n_h + 10) + 1)] + 64\lambda^2(p + 1)\Gamma_c\Gamma_h(n_h + 1)(\Gamma_h^2[n_h(40n_h^2 + 44n_h + 13) + 1]
\end{aligned}$$

$$\begin{aligned}
& \times (p-1)(p+1)^2(n_h+1)^2 + 32\lambda^2\{n_h[2n_h(16(p-1)n_h+23p-21)+15(p-1)]+p-1\}) \\
& + \Gamma_c^2(1024\lambda^4(2n_h[n_h(11pn_h-13n_h+18p-14)+6(p-1)]+p-1)+64\lambda^2(p+1)^2(n_h+1)^2 \\
& \times \Gamma_h^2\{n_h[n_h(69pn_h-71n_h+99p-95)+32(p-1)]+2(p-1)\}+(p-1)(p+1)^4(n_h+1)^4(2n_h+1) \\
& \times (3n_h+1)(7n_h+1)\Gamma_h^4\}]/\{(p-1)(n_h-n_c)[(p+1)(n_c+1)(n_h+1)+32\lambda^2(p+1)\Gamma_h(n_h+1)(4n_h+1) \\
& \times \Gamma_c^2\Gamma_h(n_c(4n_h+2)+3n_h+1)+\Gamma_c(32\lambda^2(4n_cn_h+3n_c+2n_h+1)+(p+1)^2\Gamma_h^2(n_h+1)^2 \\
& \times (4n_cn_h+2n_c+3n_h+1))\}^2}. \tag{C25}
\end{aligned}$$

- [1] R. Kosloff, *Entropy* **15**, 2100 (2013).
- [2] S. Vinjanampathy and J. Anders, *Contemp. Phys.* **57**, 545 (2016).
- [3] S. Bhattacharjee and A. Dutta, *Eur. Phys. J. B* **94**, 239 (2021).
- [4] G. Mahler, *Quantum Thermodynamic Processes: Energy and Information Flow at the Nanoscale* (Jenny Stanford, Singapore, 2014).
- [5] R. Alicki and R. Kosloff, in *Thermodynamics in the Quantum Regime* (Springer, New York, 2018), pp. 1–33.
- [6] S. Deffner and S. Campbell, *Quantum Thermodynamics* (Morgan & Claypool, Kentfield, CA, 2019).
- [7] A. T. Özdemir and Ö. E. Müstecaplıoğlu, *Turk. J. Phys.* **44**, 404 (2020).
- [8] A. C. Barato and U. Seifert, *Phys. Rev. Lett.* **114**, 158101 (2015).
- [9] P. Pietzonka and U. Seifert, *Phys. Rev. Lett.* **120**, 190602 (2018).
- [10] G. Benenti, G. Casati, and J. Wang, *Phys. Rev. E* **102**, 040103(R) (2020).
- [11] G. Guarnieri, G. T. Landi, S. R. Clark, and J. Goold, *Phys. Rev. Res.* **1**, 033021 (2019).
- [12] G. T. Landi, M. J. Kewming, M. T. Mitchison, and P. P. Potts, [arXiv:2303.04270](https://arxiv.org/abs/2303.04270).
- [13] It should be noted that, thanks to the time factor appearing in the expression for $\text{Var}(P)$, the left-hand side of Eq. (1) is dimensionless.
- [14] T. R. Gingrich, J. M. Horowitz, N. Perunov, and J. L. England, *Phys. Rev. Lett.* **116**, 120601 (2016).
- [15] J. M. Horowitz and T. R. Gingrich, *Nat. Phys.* **16**, 15 (2020).
- [16] P. Pietzonka, F. Ritort, and U. Seifert, *Phys. Rev. E* **96**, 012101 (2017).
- [17] J. M. Horowitz and T. R. Gingrich, *Phys. Rev. E* **96**, 020103(R) (2017).
- [18] P. Pietzonka, A. C. Barato, and U. Seifert, *Phys. Rev. E* **93**, 052145 (2016).
- [19] M. Poletini, A. Lazarescu, and M. Esposito, *Phys. Rev. E* **94**, 052104 (2016).
- [20] K. Proesmans and C. Van den Broeck, *Europhys. Lett.* **119**, 20001 (2017).
- [21] N. Shiraishi, [arXiv:1706.00892](https://arxiv.org/abs/1706.00892).
- [22] D. Chiuchiù and S. Pigolotti, *Phys. Rev. E* **97**, 032109 (2018).
- [23] A. C. Barato, R. Chetrite, A. Faggionato, and D. Gabrielli, *New J. Phys.* **20**, 103023 (2018).
- [24] S. Pigolotti, I. Neri, E. Roldán, and F. Jülicher, *Phys. Rev. Lett.* **119**, 140604 (2017).
- [25] L. P. Fischer, P. Pietzonka, and U. Seifert, *Phys. Rev. E* **97**, 022143 (2018).
- [26] A. Dechant and S.-I. Sasa, *Phys. Rev. E* **97**, 062101 (2018).
- [27] A. Dechant and S.-i. Sasa, *J. Stat. Mech.: Theory Exp.* (2018) 063209.
- [28] A. C. Barato and U. Seifert, *Phys. Rev. X* **6**, 041053 (2016).
- [29] K. Macieszczak, K. Brandner, and J. P. Garrahan, *Phys. Rev. Lett.* **121**, 130601 (2018).
- [30] T. Koyuk and U. Seifert, *Phys. Rev. Lett.* **125**, 260604 (2020).
- [31] J. S. Lee, J.-M. Park, and H. Park, *Phys. Rev. E* **100**, 062132 (2019).
- [32] J. P. Garrahan, *Phys. Rev. E* **95**, 032134 (2017).
- [33] T. Van Vu and Y. Hasegawa, *Phys. Rev. E* **100**, 032130 (2019).
- [34] K. Liu, Z. Gong, and M. Ueda, *Phys. Rev. Lett.* **125**, 140602 (2020).
- [35] T. R. Gingrich and J. M. Horowitz, *Phys. Rev. Lett.* **119**, 170601 (2017).
- [36] I. Di Terlizzi and M. Baiesi, *J. Phys. A* **52**, 02LT03 (2019).
- [37] J. S. Lee, J.-M. Park, and H. Park, *Phys. Rev. E* **104**, L052102 (2021).
- [38] J.-M. Park and H. Park, *Phys. Rev. Res.* **3**, 043005 (2021).
- [39] D. M. Busiello and C. E. Fiore, *J. Phys. A: Math. Theor.* **55**, 485004 (2022).
- [40] G. Francica, *Phys. Rev. E* **105**, 014129 (2022).
- [41] M. Carrega, M. Sassetti, and U. Weiss, *Phys. Rev. A* **99**, 062111 (2019).
- [42] L. M. Cangemi, M. Carrega, A. De Candia, V. Cataudella, G. De Filippis, M. Sassetti, and G. Benenti, *Phys. Rev. Res.* **3**, 013237 (2021).
- [43] L. M. Cangemi, V. Cataudella, G. Benenti, M. Sassetti, and G. De Filippis, *Phys. Rev. B* **102**, 165418 (2020).
- [44] K. Ptaszyński, *Phys. Rev. B* **98**, 085425 (2018).
- [45] B. K. Agarwalla and D. Segal, *Phys. Rev. B* **98**, 155438 (2018).
- [46] S. Saryal, H. M. Friedman, D. Segal, and B. K. Agarwalla, *Phys. Rev. E* **100**, 042101 (2019).
- [47] J. Liu and D. Segal, *Phys. Rev. E* **99**, 062141 (2019).
- [48] P. P. Potts and P. Samuelsson, *Phys. Rev. E* **100**, 052137 (2019).
- [49] T. Ehrlich and G. Schaller, *Phys. Rev. B* **104**, 045424 (2021).
- [50] M. Gerry and D. Segal, *Phys. Rev. B* **105**, 155401 (2022).
- [51] J. Liu and D. Segal, *Phys. Rev. E* **103**, 032138 (2021).
- [52] A. Rignon-Bret, G. Guarnieri, J. Goold, and M. T. Mitchison, *Phys. Rev. E* **103**, 012133 (2021).
- [53] A. M. Timpanaro, G. Guarnieri, and G. T. Landi, [arXiv:2106.10205](https://arxiv.org/abs/2106.10205).

- [54] M. Timpanaro, G. Guarnieri, G. T. Landi *et al.*, [arXiv:2108.05325](https://arxiv.org/abs/2108.05325).
- [55] D. Singh and C. Hyeon, *Phys. Rev. E* **104**, 054115 (2021).
- [56] P. Menczel, E. Loisa, K. Brandner, and C. Flindt, *J. Phys. A* **54**, 314002 (2021).
- [57] P. Bayona-Pena and K. Takahashi, *Phys. Rev. A* **104**, 042203 (2021).
- [58] T. Kerremans, P. Samuelsson, and P. Potts, *SciPost Phys.* **12**, 168 (2022).
- [59] H. J. D. Miller, M. H. Mohammady, M. Perarnau-Llobet, and G. Guarnieri, *Phys. Rev. Lett.* **126**, 210603 (2021).
- [60] L. d. S. Souza, G. Manzano, R. Fazio, and F. Iemini, *Phys. Rev. E* **106**, 014143 (2022).
- [61] S. Saryal, O. Sadekar, and B. K. Agarwalla, *Phys. Rev. E* **103**, 022141 (2021).
- [62] Y. Hasegawa, *Phys. Rev. Lett.* **125**, 050601 (2020).
- [63] Y. Hasegawa, *Phys. Rev. Lett.* **126**, 010602 (2021).
- [64] A. M. Timpanaro, G. Guarnieri, J. Goold, and G. T. Landi, *Phys. Rev. Lett.* **123**, 090604 (2019).
- [65] F. Carollo, R. L. Jack, and J. P. Garrahan, *Phys. Rev. Lett.* **122**, 130605 (2019).
- [66] A. A. S. Kalaei, A. Wacker, and P. P. Potts, *Phys. Rev. E* **104**, L012103 (2021).
- [67] T. Van Vu and K. Saito, *Phys. Rev. Lett.* **128**, 140602 (2022).
- [68] V. Holubec and T. Novotný, *J. Chem. Phys.* **151**, 044108 (2019).
- [69] M. O. Scully, K. R. Chapin, K. E. Dorfman, M. B. Kim, and A. Svidzinsky, *Proc. Natl. Acad. Sci. USA* **108**, 15097 (2011).
- [70] K. E. Dorfman, D. Xu, and J. Cao, *Phys. Rev. E* **97**, 042120 (2018).
- [71] H. E. D. Scovil and E. O. Schulz-DuBois, *Phys. Rev. Lett.* **2**, 262 (1959).
- [72] V. Singh and R. S. Johal, *Phys. Rev. E* **100**, 012138 (2019).
- [73] V. Singh, *Phys. Rev. Res.* **2**, 043187 (2020).
- [74] E. Geva and R. Kosloff, *Phys. Rev. E* **49**, 3903 (1994).
- [75] E. Geva and R. Kosloff, *J. Chem. Phys.* **104**, 7681 (1996).
- [76] E. Boukobza and D. J. Tannor, *Phys. Rev. Lett.* **98**, 240601 (2007).
- [77] E. Boukobza and D. J. Tannor, *Phys. Rev. A* **74**, 063823 (2006).
- [78] V. Singh, T. Pandit, and R. S. Johal, *Phys. Rev. E* **101**, 062121 (2020).
- [79] K. Kaur, V. Singh, J. Ghai, S. Jena, and Ö. E. Müstecaplıoğlu, *Physica A* **576**, 125892 (2021).
- [80] J. Klatzow, J. N. Becker, P. M. Ledingham, C. Weinzetl, K. T. Kaczmarek, D. J. Saunders, J. Nunn, I. A. Walmsley, R. Uzdin, and E. Poem, *Phys. Rev. Lett.* **122**, 110601 (2019).
- [81] Indeed, by direct inspection, one can consider the following more abstract rules to define a unified model. Consider an engine working among three levels, $|g\rangle$, $|0\rangle$, and $|1\rangle$. We then define the hot reservoir to connect level $|g\rangle$ with level $|1\rangle$ and the cold reservoir to connect level $|0\rangle$ with level $|g\rangle$. Finally, the driving is between level $|0\rangle$ and $|1\rangle$. Given these rules, it is immediate to recognize that model I corresponds to the case with $\omega_g < \omega_0 < \omega_1$, while model II corresponds (up to an inessential relabeling) to the case $\omega_1 < \omega_0 < \omega_g$.
- [82] R. Kosloff and Y. Rezek, *Entropy* **19**, 136 (2017).
- [83] S.-W. Li, M. B. Kim, G. S. Agarwal, and M. O. Scully, *Phys. Rev. A* **96**, 063806 (2017).
- [84] C. C. Gerry and P. L. Knight, *Introductory Quantum Optics* (Cambridge University, New York, 2005).
- [85] R. J. Glauber, *Phys. Rev.* **130**, 2529 (1963).
- [86] M. Esposito, K. Lindenberg, and C. Van den Broeck, *Phys. Rev. Lett.* **102**, 130602 (2009).
- [87] A. Parmeggiani, F. Jülicher, A. Ajdari, and J. Prost, *Phys. Rev. E* **60**, 2127 (1999).
- [88] T. E. Humphrey, R. Newbury, R. P. Taylor, and H. Linke, *Phys. Rev. Lett.* **89**, 116801 (2002).
- [89] T. E. Humphrey and H. Linke, *Phys. Rev. Lett.* **94**, 096601 (2005).
- [90] M. F. O'Dwyer, T. E. Humphrey, and H. Linke, *Nanotechnology* **17**, S338 (2006).
- [91] B. Cleuren, C. Van den Broeck, and R. Kawai, *Phys. Rev. E* **74**, 021117 (2006).
- [92] M. Bruderer, L. D. Contreras-Pulido, M. Thaller, L. Sironi, D. Obreschkow, and M. B. Plenio, *New J. Phys.* **16**, 033030 (2014).
- [93] G. Schaller, *Open Quantum Systems Far from Equilibrium* (Springer, New York, 2014), Vol. 881.
- [94] See Supplemental Material at <http://link.aps.org/supplemental/10.1103/PhysRevA.108.032203> for a MATHEMATICA file.